ACS Catalysis

Research Article

pubs.acs.org/acscatalysis

Redispersion of Gold Multiple-Twinned Particles during Liquid-Phase Hydrogenation

Christiane Kartusch,[†] Frank Krumeich,[†] Olga Safonova,[‡] Urs Hartfelder,[†] Martin Makosch,[†] Jacinto Sá,[‡] and Jeroen A. van Bokhoven*[,†,‡]

[†]Institute for Chemical and Bioengineering, ETH Zürich, Wolfgang-Pauli Strasse 10, 8093 Zurich, Switzerland

[‡]Laboratory for Catalysis and Sustainable Chemistry, Paul Scherrer Institute, 5232 Villigen PSI, Switzerland

ABSTRACT: Controlling the particle size of supported metal catalysts is essential to achieving active, selective, and stable catalysts. High-resolution electron microscopy has revealed that large Au particles (~8 nm), supported on titania and if multiple-twinned, broke up into small particles (2−3 nm) during liquid-phase hydrogenation. Multiple-twinned Au particles, obtained after gas-phase reduction of as-prepared Au/TiO_2 at elevated temperature, break up into smaller particles. EXAFS confirmed that the multiple-twinned particles were agglomerates of smaller particles. In contrast, calcination caused a strong interaction between Au and titania and the formation of mainly single crystalline Au particles (4 to 5 nm), which were relatively stable during liquid-phase hydrogenation. Reduction and calcination lead to gold particles that are fundamentally different.

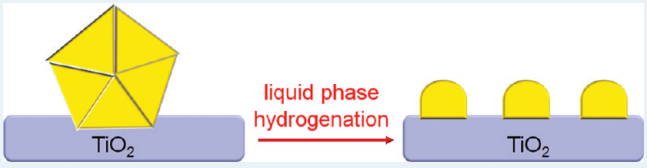

KEYWORDS: *gold, titania, multiple-twinned particles, redispersion, electron microscopy, X-ray absorption spectroscopy*

INTRODUCTION

Redispersion of supported metal particles is a highly interesting topic, in particular because it is the reverse of sintering, the main process of catalyst deactivation.[1−7] Deactivation through sintering can be restored by redispersion of the supported metal particles under the appropriate conditions.[2−6] Redispersion takes place by complex physical and chemical processes[8] and is a function of temperature, atmosphere, time, and support. It is also strongly influenced by the metal and its loading or promotors (or both) as well as by catalyst preparation.[1,9−11] Redispersion has been reported for supported metals such as Pt,[3,5,12−18] Pd,[6,19−21] Rh,[22−27] Co,[28−31] Ni,[32−34] and Ag.[35,36] The mechanisms differ considerably, depending on the metal, the support, their interaction, and the applied conditions. For the above-mentioned metals, redispersion has been applied successfully for catalyst regeneration for many years, whereas only a few recent studies have focused on the redispersion of supported gold particles.[37−42]

We report the redispersion of Au/TiO_2 catalysts during high-pressure liquid-phase hydrogenation of nitroaromatic compounds. Gold catalyzes a number of hydrogenation reactions, among them hydrogenation of alkenes,[43,44] alkadiens,[45−48] alkynes,[49−52] α,β-unsaturated carbonyl compounds,[53−56] and nitro compounds.[57−59] The size of supported Au particles strongly affects catalytic activity. Although bulk gold is catalytically inactive, the high activity of Au nanoparticles was attributed to the greater proportion of low-coordinated Au sites,[60−62] electronic effects,[56,63] and the involvement of the metal−support interface in the activitation of reactants.[64,65] Furthermore, an efficient interaction with the support is required.[66] To date, the influence of the support is not well understood. However, in the hydrogenation of nitroaromatic compounds in particular, the use of TiO_2 often led to significantly higher activity and selectivity compared with other metal oxide supports.[57,67−72] The mechanism of H_2 splitting on Au/TiO_2 is a subject of debate, and various models exist.[65,73−80] It is generally accepted that the reaction occurs at the metal−support interface. The adsorption of nitrobenzene at this interface is assumed to make the catalysts selective.[74] Corma et al. have shown that Au/TiO_2 selectively reduced the nitro group in the presence of various reducible functional groups such as double bonds, carbonyl, amide, or nitrile groups under mild conditions (100−120 °C, 10 bar H_2).[57] The redispersion of Au/TiO_2 during liquid-phase hydrogenation of 4-nitrobenzaldehyde, nitrobenzene, and nitrosobenzene was determined by electron microscopy and EXAFS. The most direct methods, TEM and STEM, provide real images of the particles, which give an impression of the homogeneity of a sample. EXAFS on the other hand, is a bulk technique, which provides average particle sizes of a relatively large volume.[81]

EXPERIMENTAL SECTION

Catalyst Preparation. Au/TiO_2 was prepared through deposition precipitation with urea.[82] To prepare 0.7 wt % Au/TiO_2, 0.086 g of $HAuCl_4 \cdot H_2O$ (49 wt % Au, ABCR Chemicals) was dissolved in 600 mL deionized H_2O. Then 6.0 g of TiO_2 (Aeroxide P25, Acros Organics) and 1.8 g of urea (puriss, Riedel-de Haën) were added to the stirred mixture, which was heated to 80 °C and stirred for another 16 h in a closed Teflon

Received: January 30, 2012
Revised: May 11, 2012
Published: May 14, 2012

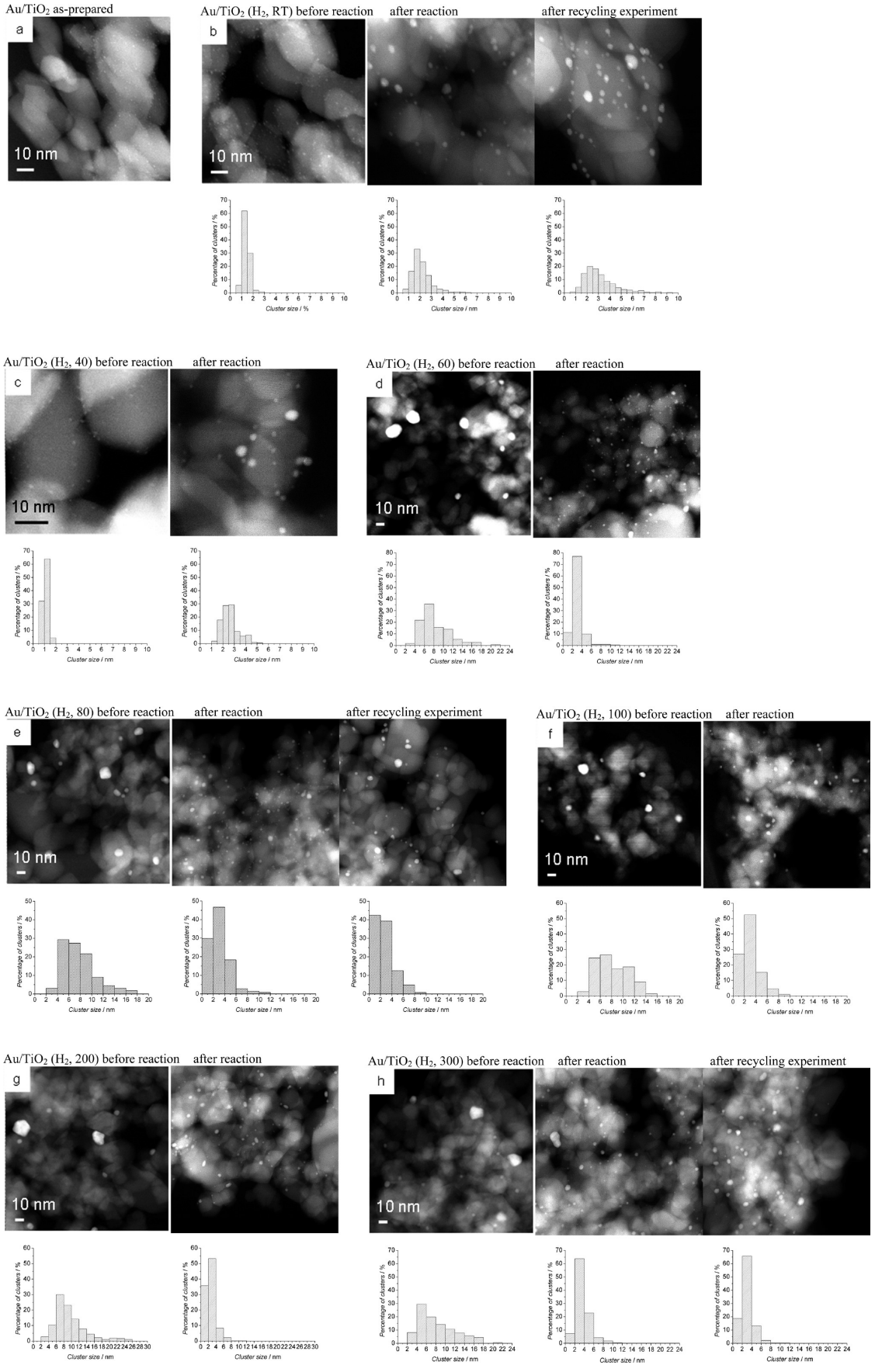

Figure 1. continued

dx.doi.org/10.1021/cs300075k | *ACS Catal.* 2012, 2, 1394−1403

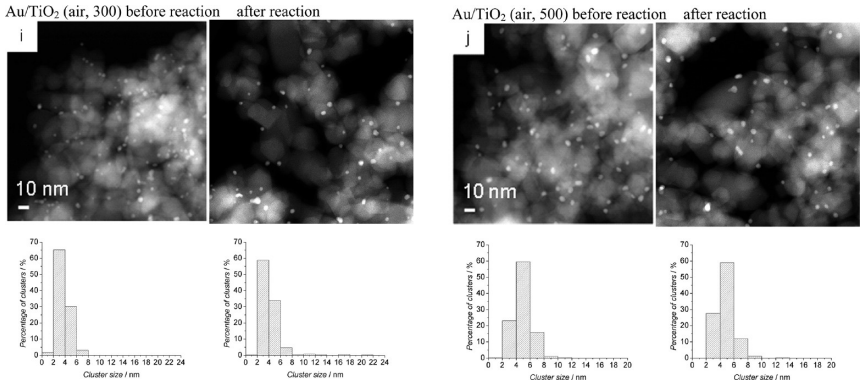

Figure 1. Representative HAADF−STEM micrographs and particle size distributions of as-prepared Au/TiO_2 and of differently pretreated Au/TiO_2 before and after reaction in the liquid-phase hydrogenation of 4-nitrobenzaldehyde to 4-aminobenzaldehyde at 100 °C and 10 bar H_2. For Au/TiO_2 pretreated in H_2 at room temperature and 80 and 300 °C, TEM micrographs and particle size distributions after recycling experiments are given.

vessel. After cooling to room temperature, the filtrate was washed five times with deionized water to remove residual chloride ions. To ensure the removal of chloride, $AgNO_3$ solution (1M) was added to the filtrate. Precipitation of AgCl was not observed. The yellowish product was dried at room temperature under vacuum in the dark for 48 h. The resulting catalyst was referred to as "as-prepared". If it was not used right after synthesis, then it was stored at −18 °C in the dark. With the aim of obtaining gold particles of different sizes and of investigating the influence of different pretreatment conditions, as-prepared Au/TiO_2 was reduced in a flow of 5% H_2/He (100 mL/min) at room temperature for 45 min and at different temperatures (40, 60, 80, 100, 150, 200, 300 °C) for 20 min at a heating rate of 2 °C/min; it was then cooled to room temperature under the same conditions. Alternatively, as-prepared Au/TiO_2 was calcined in a flow of air (100 mL/min) at 300, 400, and 500 °C and a heating rate of 2 °C/min and a dwell time of 30 min and then cooled to room temperature under the same stream of air. Pretreated catalysts were stored at −18 °C in the dark. They were pretreated right before the start of the kinetic experiments.

Kinetic Experiments. The liquid-phase hydrogenation of 4-nitrobenzaldehyde, nitrobenzene, nitrosobenzene, and benzaldehyde was performed in stainless steel autoclaves with a volume of 50 mL (Premex Reactor AG, Lengnau, Switzerland), which were equipped with a gas inlet and outlet, a sample port, a thermocouple, external heating, and readout for temperature and pressure. Stirring was performed with a magnetic stirrer.

To perform a kinetic experiment, the catalyst, the substrate, THF or toluene as the solvent, and mesitylene as the internal standard were placed in the reactor. In most cases, 0.06 g of catalyst, 0.06 g of substrate, 25 g of solvent, and 0.14 mL of internal standard were used. In general, samples of around 1 mL were taken at room temperature at 0, 10, 30, 60, 120, 180, and 240 min by means of a sample tube. After filtration to remove the residual catalyst, the concentration of the reactants and products was quantified by gas chromatography on an Agilent 7820A gas chromatograph equipped with a HP5-MS column. The column was initially kept at 80 °C for 2 min and then heated to 300 °C at a rate of 20 °C/min. If required, the reaction was continued overnight until full conversion was reached. Before the reaction started, residual air was removed by flushing the reactor three times with hydrogen to 10 bar while stirring, followed by venting. The autoclave was then pressurized with hydrogen to 10 bar and heated to the reaction temperature of 100 °C without stirring. At 100 °C, stirring was started and the reaction time was set at zero. The main product of the reduction of 4-nitrobenzaldehyde−4-aminobenzaldehyde is unstable because the aldehyde and the amino groups react by condensation to imines, which can reduce further. These products were not detected directly by GC because they were too heavy to be brought into the gas phase. They were found after reaction in the form of an orange solid attached to the wall of the autoclave, the amounts of which were determined from the carbon balance.

Characterization. *Atomic Absorption Spectroscopy and ICP-OES Spectroscopy.* The Au content of Au/TiO_2, determined by AAS with a Varian SpectrAA 220 FS spectrometer, was 0.78 wt %. The Ti content of Au/TiO_2 was determined by ICP-OES using a Varian VISTA PRO AX spectrometer. Sample preparation was performed by microwave-assisted digestion by adding 1 mL of nitric acid, 2 mL of hydrofluoric acid, and 3 mL of hydrochloric acid to 40 mg of catalyst to determine the Au content and to 10 mg of catalyst to determine the Ti content.

Electron Microscopy. Electron microscopy measurements of Au/TiO_2 catalysts after pretreatment and after reaction were performed on a HD2700CS (Hitachi, aberration-corrected dedicated scanning transmission electron microscope (STEM), cold FEG, 200 kV) or a Tecnai F30 ST (FEI, FEG, 300 kV). The high resolution of HD2700CS (shown to be better than 0.1 nm) is due to a probe corrector (CEOS) that is incorporated in the microscope column between the condenser lens and the probe-forming objective lens so that a beam diameter of ∼0.1 nm is achieved.[83] A special bright field setting enables the determination of the highly resolved phase-contrast STEM (PC-STEM) images (similar to HRTEM) without delocalization artifacts. With high-angle annular dark field detectors (HAADF) attached to both microscopes, the intensity of incoherently scattered electrons is measured, leading to images dominated by atomic number (Z) contrast;[84] the Au particles appear as bright patches.

After reaction, the catalysts were recovered by filtering and washing several times with THF and then drying at room temperature under vacuum. For the (scanning) transmission electron microscopy, the catalyst material was dispersed in ethanol, and a few drops of the suspension were placed on a perforated carbon foil supported on a copper grid. Three hundred particles were usually counted in the HAADF−STEM images to determine the particle size distributions. For Au/

dx.doi.org/10.1021/cs300075k | ACS Catal. 2012, 2, 1394−1403

Table 1. Particle Size before and after Reaction and Catalytic Activity and Selectivity of Differently Pretreated Au/TiO_2 in the Liquid-Phase Hydrogenation of 4-Nitrobenzaldehyde to 4-Aminobenzaldehyde at 100 °C and 10 bar H_2

entry	pretreatment temp/°C	pretreatment gas	rate at 50% conversion/ mmol/(g_{Au}·s)	selectivity at 100% conversion/%	HAADF−STEM mean particle size before reaction/nm	HAADF−STEM mean particle size after reaction/nm
1	as-prepared				0.8 ± 0.2	
2	25	H_2	0.11 ± 0.08	80	1.4 ± 0.3	2.1 ± 0.8
3[a]			0.05	76	2.1 ± 0.8	3.0 ± 1.4
4	40	H_2	0.05 ± 0.01	70	1.1 ± 0.2	2.7 ± 0.6
5	60	H_2	0.11 ± 0.03	75	8.2 ± 3.2	3.0 ± 1.2
6	80	H_2	0.08 ± 0.02	55	7.6 ± 2.9	3.0 ± 1.7
7[a]			0.04	75	3.0 ± 1.7	2.7 ± 1.5
8	100	H_2	0.08 ± 0.02	75	8.1 ± 2.7	3.0 ± 1.5
9	150	H_2	0.10 ± 0.02	75		
10	200	H_2	0.09 ± 0.03	75	9.5 ± 4.1	2.5 ± 1.2
11	300	H_2	0.08 ± 0.03	67	8.2 ± 3.8	2.8 ± 1.2
12[a]			0.04	15	2.8 ± 1.2	3.5 ± 1.4
13	300	air	0.11 ± 0.04	75	3.7 ± 1.0	4.4 ± 3.7
14	400	air	0.07 ± 0.01	70		
15	500	air	0.06 ± 0.01	70	4.8 ± 1.2	4.7 ± 1.2

[a]Recycling experiment: After the reaction, the used catalyst was filtered, washed several times with THF, dried at room temperature, and then reused in the recycling experiment. Except for the recycling experiments, all the reactions were performed three times; the average results are given.

TiO_2 pretreated in H_2 between 60 and 300 °C, all the measured particles (about 100) were taken into account.

X-ray Absorption Spectroscopy. XAS measurements at the Au L_3 edge were performed at the SuperXAS beamline at the Swiss Light Source (Paul Scherrer Institute, Villigen, Switzerland) in transmission mode by measuring the intensity of the beam before and after the sample by ionization chambers. The Swiss Light Source has a ring energy of 2.4 GeV, a ring current of 400 mA, and a magnetic field of 2.9 T and is operated in the "top-up" injection mode. The incident energy was focused with two mirrors and monochromatized using a double crystal monochromator equipped with a pair of Si(111) crystals. About 30 mg of catalyst was used to prepare self-supporting pellets with a diameter of 5 mm to obtain optimal transmission properties. The pellets were placed in a sample holder and measured at room temperature. One spectrum per sample was recorded in the energy range of 11.8−13.0 keV with a scan time of 45 min. The EXAFS data were analyzed using the Athena and Artemis software packages. The first shell was fitted in R space ($1.5 < R < 3.5$ Å) after Fourier transformation ($3 < k < 13$ Å^{-1}) using a k weighting of 2. Average particle sizes were determined from the coordination numbers using established methods and assuming spherical particles.[85]

RESULTS

Figure 1 shows representative HAADF−STEM micrographs and the corresponding particle size distributions of Au/TiO_2 as-prepared, after pretreatment in H_2 at room temperature and 40, 60, 80, 100, 200, and 300 °C as well as after calcination in air at 300 and 500 °C. Figure 1 presents representative HAADF−STEM micrographs and particle size distributions of the catalysts after the reaction. Table 1 lists the catalytic activity and selectivity in the liquid-phase hydrogenation of 4-nitrobenzaldehyde and the average Au particle sizes determined by HAADF−STEM. All results in Figure 1 and Table 1 were obtained from the same batch of Au/TiO_2, and each experiment was repeated twice, with the exception of the recycling experiments. The bright dots in the HAADF−STEM micrographs correspond to the Au particles (Z contrast). As-prepared Au/TiO_2 (Figure 1a, Table 1 entry 1) contained the smallest Au particles, with a mean size of 0.8 nm and a narrow size distribution. Au/TiO_2, pretreated in H_2 at RT (Figure 1b, Table 1 entry 2) and 40 °C (Figure 1c, Table 1 entry 4), had slightly larger particles of around 1.4 and 1.1 nm, respectively, which were also dispersed uniformly with a narrow distribution. Pretreatment in H_2 between 60 and 300 °C led to the formation of large particles of ∼8−10 nm, heterogeneously distributed on the support. After pretreatment in air at 300 to 500 °C, Au particles (4−5 nm) formed; they were more or less homogeneously distributed on the support.

Taking into account the large differences in the initial particle sizes (1−10 nm), the differences in the catalytic activity were relatively small. After reduction in H_2 at 60 to 300 °C as well as calcination at 300 °C, the catalysts exhibited similar rates (0.08−0.11 mmol/(g_{Au}·s)) at 50% conversion. The lower activity of Au/TiO_2, pretreated in H_2 at 40 °C and the large standard deviation of the rate of Au/TiO_2 pretreated at RT were probably due to incomplete reduction of the oxidic gold during pretreatment. This was indicated by the yellowish color of the catalysts after pretreatment, similar to as-prepared Au/TiO_2, whereas fully reduced Au/TiO_2 is usually purple. The oxidic Au species then reduced under reaction conditions, which occurs in an uncontrolled and, thus, nonreproducible manner without contributing to the catalytic activity. Among the calcined samples, the catalytic activity decreased slightly with increasing calcination temperature.

The selectivity to the desired product 4-aminobenzaldehyde was comparable for all catalysts, being around 75% at full conversion.

To determine whether the average particle size and size distribution changed depending on the reaction conditions, the catalysts after reaction were subjected to HAADF−STEM measurements (Figure 1, Table 1). The particle size distribution of Au/TiO_2, calcined at 500 °C, hardly changed under the reaction conditions (Figure 1j, Table 1 entry 15). Au particles in Au/TiO_2 calcined at 300 °C sintered slightly during the reaction. Sintering of Au nanoparticles also occurred for Au/TiO_2 pretreated in H_2 at RT and 40 °C. The average particle size increased from ∼1 nm to 2 and 3 nm, respectively.

dx.doi.org/10.1021/cs300075k | ACS Catal. 2012, 2, 1394−1403

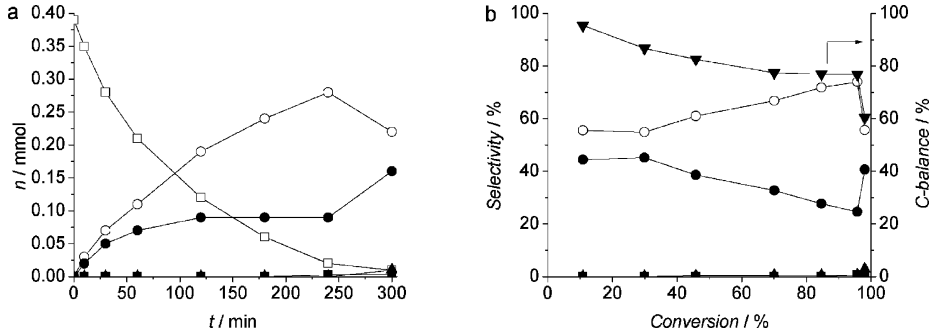

Figure 2. Conversion (a) and selectivity (b) plot for the hydrogenation of 4-nitrobenzaldehyde with Au/TiO_2 reduced in 5% H_2/He at 80 °C: (□) 4-nitrobenzaldehyde, (○) 4-aminobenzaldehyde, (▲) 4-aminotoluene, (■) 4-aminobenzylalcohol, (●) condensation products, (▼) C-balance (0.4 mmol substrate, 10 bar H_2, 100 °C).

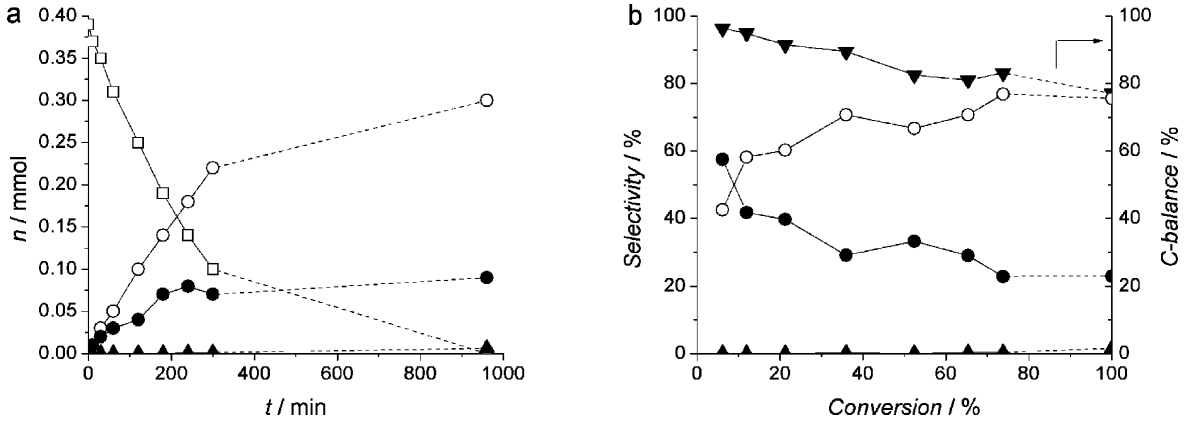

Figure 3. Conversion (a) and selectivity (b) plot for the hydrogenation of 4-nitrobenzaldehyde with recycled Au/TiO_2 (previously reduced in 5% H_2/He at 80 °C): (□) 4-nitrobenzaldehyde, (○) 4-aminobenzaldehyde, (▲) 4-aminotoluene, (●) condensation products, (▼) C-balance (0.4 mmol substrate, 10 bar H_2, 100 °C).

Au/TiO_2 pretreated in H_2 from 60 to 300 °C changed significantly under the reaction conditions. The HAADF−STEM micrographs after the reaction show a large number of small particles, in contrast to the large particles before the reaction. For all the catalysts, the average Au particle size decreased from ∼8−10 nm to 2−3 nm. After pretreatment, none of the particles were smaller than 2 nm; thus, the catalysts after reaction contained significant numbers of particles in this size range. Thus, Au particles supported on TiO_2 after pretreatment in H_2 between 60 and 300 °C redispersed under the applied reaction conditions. These results were reproduced with two new batches of Au/TiO_2 under two different pretreatment conditions (reduction in H_2 at 80 and 300 °C).

To determine whether the small particles formed because of leaching of Au and redeposition during reaction, the Au and Ti contents of some of the catalysts were determined before and after the reaction by AAS and ICP-OES. Around 8% leaching of Au occurred. If leaching were the reason for the formation of small particles, then the gold content would have decreased to a much larger extent. Hot filtration experiments are in line with the results of elemental analysis. After 17 h, there was 20% conversion of 4-nitrobenzaldehyde after hot filtration, compared with 6% conversion in the control experiments and full conversion in the respective catalytic experiments, indicating that the activity of the liquid phase is very low.

Figure 2 shows the conversion and selectivity plot of the liquid-phase hydrogenation of 4-nitrobenzaldehyde over Au/TiO_2 pretreated in H_2 at 80 °C. In addition to the main product 4-aminobenzaldehyde, significant amounts of oligomeric and polymeric compounds formed as a result of the well-known condensation of primary amines and aldehydes to imines. These products were not detected directly by gas chromatography but were determined by the carbon balance (Figure 2-b). Furthermore, small amounts of 4-aminotoluene and 4-aminobenzylalcohol (<5%) were detected by gas chromatography. Within 300 min, 4-nitrobenzaldehyde was fully converted.

Some catalysts—namely, Au/TiO_2 pretreated in H_2 at RT, 80 °C, and 300 °C—were reused in the hydrogenation of 4-nitrobenzaldehyde. The recycled catalysts, obtained by filtering, washing with THF, and then drying were only half as active as the fresh ones. Figure 3 shows the conversion and selectivity plot of the hydrogenation of 4-nitrobenzaldehyde over recycled Au/TiO_2, initially reduced in H_2 at 80 °C. The selectivity to 4-aminobenzaldehyde at full conversion was slightly higher with the recycled catalyst than with the fresh one as a result of the formation of fewer condensation products. Like the fresh sample, the recycled catalyst, too, produced only low amounts (<5%) of the secondary products 4-aminotoluene and 4-aminobenzylalcohol.

The particle size distributions hardly changed during the recycling experiments; thus, sintering cannot have caused the deactivation. The decrease in catalytic activity is probably due to the poisoning of the catalyst surface by reaction intermediates, deposition of carbonaceous species,[86] or both.

To corroborate the results of HAADF−STEM, we performed EXAFS measurements at the Au L_3 edge of Au/TiO_2 before and after reaction using a new batch of Au/TiO_2.

dx.doi.org/10.1021/cs300075k | ACS Catal. 2012, 2, 1394−1403

Figure 4 presents the XANES spectra of Au/TiO_2, after pretreatment in H_2 at 80 °C and after hydrogenation of 4-nitrobenzaldehyde and of Au foil. The main features in the spectrum, after pretreatment and after reaction, matched those of the Au foil; thus, the Au nanoparticles were fully reduced.

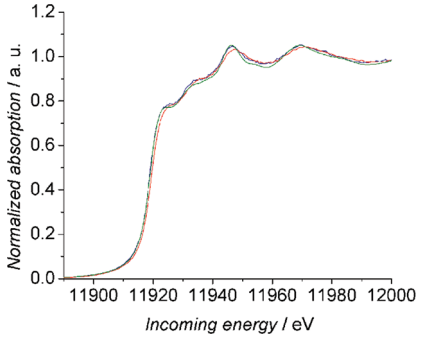

Figure 4. XANES spectra at the Au L_3 edge of Au/TiO_2, pretreated in H_2 at 80 °C (blue) and after hydrogenation of 4-nitrobenzaldehyde at 100 °C and 10 bar H_2 (red), and of Au foil (green).

Figure 5 shows the EXAFS functions (a) and Fourier transforms (b). The quality of the EXAFS data was good up to at least 12 $Å^{-1}$. The amplitude of the oscillations and, thus, the intensity of the Fourier transforms were highest for the Au foil, followed by Au/TiO_2 after pretreatment and Au/TiO_2 after reaction, clearly indicating differences in the structure. The intensity of the EXAFS oscillations is directly proportional to the average number of scattering atoms surrounding the central atom and, hence, the average particle size. The data of Au/TiO_2 after pretreatment and after reaction were fitted to the Au−Au coordination numbers of 9.3 and 8.0, respectively (Table 2). Table 2 gives the mean particle size of the catalyst before and after reaction as determined from the EXAFS coordination number and assuming spherical particles[85] as well as the HAADF−STEM mean particle sizes. The EXAFS mean particle sizes before and after reaction were 2.1 and 1.4 nm, respectively. Although the trend is the same, these results largely deviate from the HAADF−STEM mean particle sizes of 7.1 and 2.5 nm.

The smaller particle sizes revealed by EXAFS may be due to the fact that the large particles revealed by HAADF−STEM are not single crystal particles but aggregates of smaller particles.

Figure 6 shows zoomed phase-contrast (PC) STEM micrographs of Au particles supported on TiO_2 after pretreatment in H_2 at 300 °C. The size of the particles was between 9 and 13 nm. The particles were not single crystals but multiply twinned particles with clearly visible grain boundaries.[87−89] In each particle, crystalline segments of different shapes are joined in different ways. The EXAFS analysis probably probes the size of the individual grains. The structure of the small particles after reaction changed considerably under the electron beam; it was therefore impossible to determine their structure. This behavior

Table 2. Coordination Numbers of Au/TiO_2 Pretreated in H_2 at 80 °C before and after Hydrogenation of 4-Nitrobenzaldehyde at 100 °C and 10 bar H_2 and Corresponding Average Au Particle Sizes Determined by EXAFS and HAADF−STEM

sample	CN	EXAFS mean particle size/nm[a]	TEM mean particle size/nm
Au/TiO_2 before reaction	9.3	2.1	7.1 ± 3.6
Au/TiO_2 after reaction	8	1.4	2.5 ± 0.8

[a]EXAFS mean particle size[85] determined on the basis of the assumption of spherical particles.

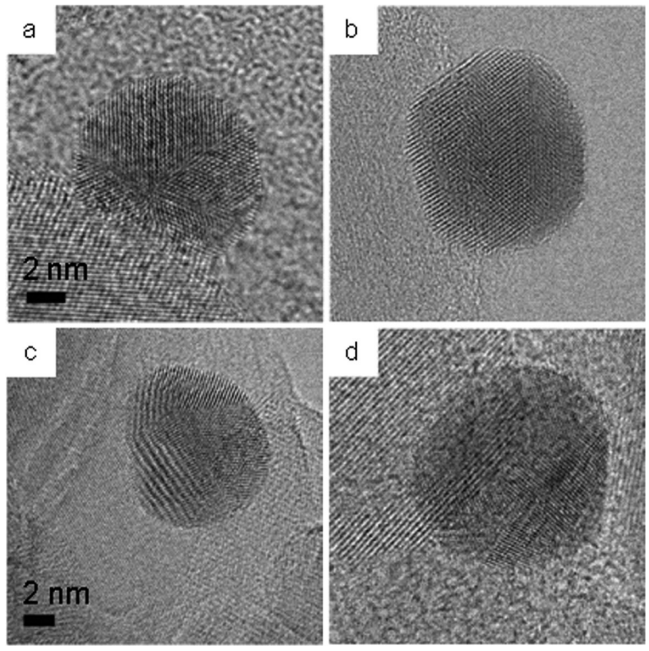

Figure 6. PC-STEM micrographs of Au nanoparticles supported on TiO_2 after pretreatment in H_2 at 300 °C.

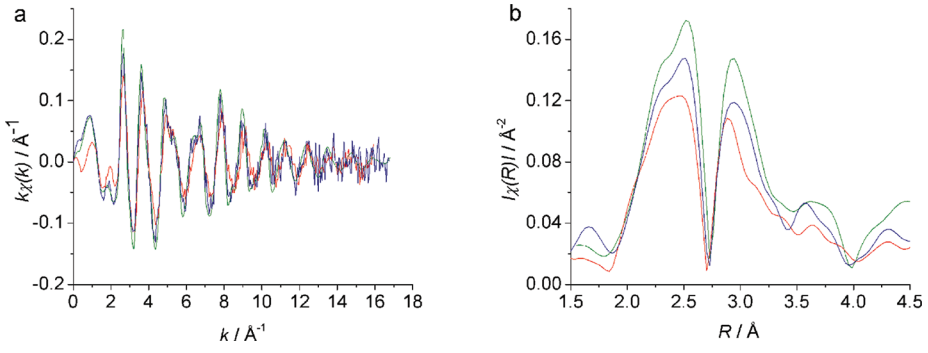

Figure 5. EXAFS functions (a) and corresponding Fourier transforms (b) of Au/TiO_2 after pretreatment in H_2 at 80 °C (blue) and after hydrogenation of 4-nitrobenzaldehyde at 100 °C and 10 bar H_2 (red) as well as of gold foil (green).

dx.doi.org/10.1021/cs300075k | ACS Catal. 2012, 2, 1394−1403

was also observed by Iijima et al.[90] and by Zhang et al.[91] for Au particles of 3 nm supported on carbon.

Figure 7 shows representative PC-STEM micrographs of Au particles supported on TiO_2 after calcination at 500 °C with

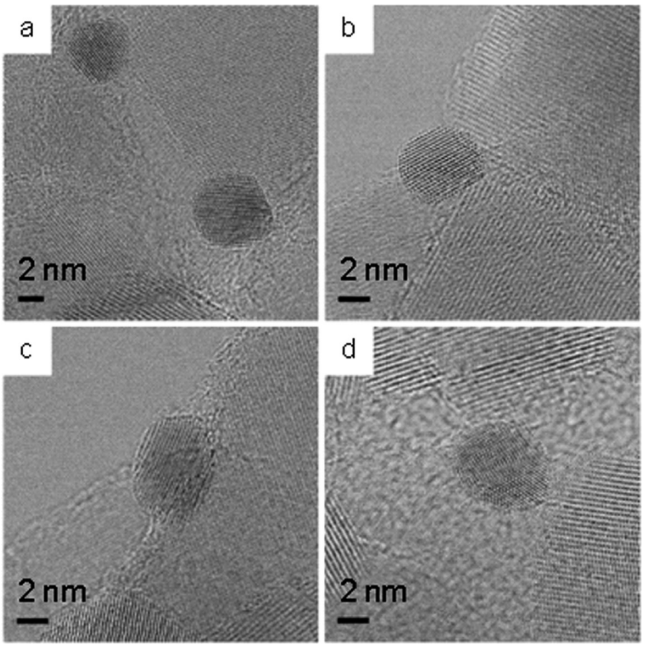

Figure 7. PC-STEM micrographs of Au nanoparticles supported on TiO_2 after pretreatment in air at 500 °C.

sizes between 5 and 10 nm. In contrast to the Au particles after pretreatment in H_2, most of the Au particles were single crystals (Figure 7a, b, c), only some (Figure 7d) were multiple twins.

To determine whether redispersion of gold might be restricted to 4-nitrobenzaldehyde, another batch of Au/TiO_2 was tested in the hydrogenation of nitrobenzene, nitrosobenzene, and benzaldehyde. The catalyst was pretreated in H_2 at 80 °C. Table 3 presents the conversion of the substrates

Table 3. Mean Particle Size of Au/TiO_2 after 240 min Hydrogenation of Nitrobenzene, Nitrosobenzene, and Benzaldehyde, Respectively, at 100 °C and 10 bar H_2

entry	substrate	conversion/%	mean particle size/nm
1	Au/TiO_2 (H80)[a]		10.5 ± 5.2
2	nitrobenzene	96	2.5 ± 0.8
3	nitrosobenzene	100	2.5 ± 0.9
4	benzaldehyde	15	7.0 ± 3.2

[a]This catalyst was used in all three experiments. The reaction time for all substrates was 240 min.

and the corresponding mean particle size of Au/TiO_2 after 240 min, at 100 °C, and 10 bar H_2. The mean particle size of Au/TiO_2 after pretreatment was 10.5 nm with a broad size distribution. After 240 min, the conversion of nitrobenzene was 96%. With nitrosobenzene, which is a reactive intermediate in the reduction of nitrobenzene to aniline, full conversion was reached. The Au particle size after reaction of both substrates was narrowly distributed at around 2.5 nm. Thus, redispersion also occurred in the presence of nitrobenzene and nitrosobenzene. On the other hand, only 15% of benzaldehyde converted under the applied conditions. The Au particle size decreased only slightly to around 7 nm. This suggests that the nitro group, reaction intermediates, or aniline might play an active role in the redispersion of gold during reaction.

To investigate the point at which the redispersion took place, the hydrogenation of nitrobenzene over Au/TiO_2 pretreated in H_2 at 80 °C was stopped at different conversion levels to determine the particle size. Figure 8 shows the mean particle

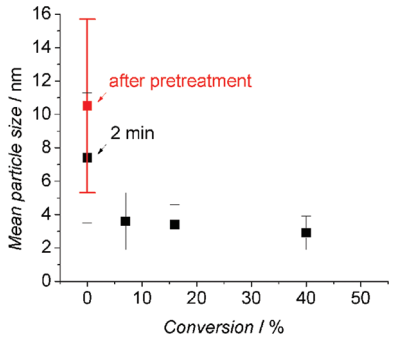

Figure 8. Mean particle size of Au/TiO_2 (pretreatment: H_2, 80 °C) at different conversion levels during the hydrogenation of nitrobenzene at 100 °C and 10 bar H_2 plotted against the conversion.

size plotted against the conversion. The error bars correspond to the standard deviation of the mean particle size. After pretreatment, the mean Au particle size was 10.5 nm. After 2 min of reaction (i.e. while heating in H_2 to the desired reaction temperature of 100 °C), it was 7.4 nm. Virtually no conversion of nitrobenzene was detected by GC. After 5 min, the reaction temperature of 100 °C was reached. The conversion of nitrobenzene was 7%, and the mean Au particle size was 3.6 nm. After 15 min, at a conversion level of 16%, the mean Au particle size was 3.4 nm. After 40% conversion (30 min), the mean Au particle size was 2.9 nm. With increasing conversion and decreasing mean particle size, the size distribution became narrower, as illustrated by the decreasing standard deviations. In summary, redispersion occurred fast at the beginning of the reaction at conversion levels <10%.

Furthermore, we detected whether redispersion occurred only in the presence of the reactants or the intermediates (or both) or in pure solvents, as well as the influence of the gas atmosphere and temperature. Therefore, another batch of Au/TiO_2, pretreated in H_2 at 80 °C, was subjected to different reaction conditions and times; and subsequently, the Au particle size was determined by TEM (Table 4). THF and

Table 4. Mean Particle Size of Au/TiO_2, Pretreated in H_2 at 80 °C under Different Reaction Conditions

entry	solvent	reactant	gas (p)/ bar	T/°C	mean p. size after 2 min/nm	mean p. size after 30 min/nm
1					8.2[a] ± 4.7	
2	THF		H_2 (10)	100	3.4 ± 10.1	7.4 ± 2.7
4	THF		H_2 (10)	25	3.9 ± 1.5	3.0 ± 1.2
5	THF		He (7)	100	2.9 ± 1.1	3.4 ± 1.0
6	THF		He (7)	25	10.3 ± 6.6	12.6 ± 8.4

[a]Mean particle size of Au/TiO_2 after pretreatment in a flow of H_2 at 80 °C. This catalyst was used in the experiments listed in this table.

dx.doi.org/10.1021/cs300075k | ACS Catal. 2012, 2, 1394–1403

toluene solvents were tested at 25 and 100 °C, in 10 bar H_2 and 7 bar He. The experiments were stopped after 2 and 30 min, respectively, to determine time-dependent changes. Both solvents yielded similar results; therefore, only those of THF are presented in Table 4. In H_2, the Au particles redispersed both at RT and at 100 °C. Thus, in H_2, redispersion did not depend on temperature in the investigated temperature range. In He, Au supported on TiO_2 redispersed at 100 °C but not at RT, indicating that in inert gas, redispersion was dependent on temperature. The mean Au particle size in H_2 at 100 °C was 3 nm after 2 min and 7 nm after 30 min. Thus, redispersion was followed by sintering. These results show the dynamic changes of the catalyst under varying conditions.

DISCUSSION

After pretreatment of as-prepared Au/TiO_2, in a flow of H_2 at 60−300 °C, large Au particles (8−10 nm) with broad size distributions formed. The Au particles were fully reduced, as revealed by EXAFS measurements of Au/TiO_2 after pretreatment at 80 °C and after reaction. In situ EXAFS measurements of Bus et al.[92] showed a complete reduction of Au species supported on titania at 60 °C under the same conditions. The large particles probably formed after reduction of the Au precursor due to the elevated temperature. It was found that pretreatment of Au/TiO_2 in H_2 at RT for 45 min resulted in fully reduced Au particles of ∼1.5 nm.[92] H_2O may have formed during the reduction of the Au precursor and may have facilitated the formation of large particles. UHV studies about the nucleation of Au particles on mildly hydroxylated and slightly reduced TiO_2(110) surfaces showed that water binds to oxygen vacancy centers, which otherwise act as nucleation sites for Au.[93,94]

For all samples pretreated in H_2 between 60 and 300 °C, large particles broke up into small particles of ∼2−3 nm in the liquid phase during hydrogenation of 4-nitrobenzaldehyde, nitrobenzene, and nitrosobenzene at 100 °C and 10 bar H_2 as well as in pure solvents such as THF and toluene in the presence of H_2 at room temperature and 100 °C and in an inert gas, but only at 100 °C. Thus, the large Au particles broke apart under reducing conditions. Significant numbers of particles smaller than 2 nm formed; they are considered to be highly active, whereas after pretreatment, the catalysts did not contain particles smaller than 2 nm. There was no redispersion of large Au particles on Au/Al_2O_3.[95] In contrast to the reduced samples, Au particles in calcined Au/TiO_2, with the majority of the particles in the size range between 2 and 8 nm, did not break apart under the reaction conditions. On the contrary, the particle size distribution of Au/TiO_2, calcined at 500 °C, hardly changed during hydrogenation; Au particles in Au/TiO_2 after calcination at 300 °C sintered slightly under the reaction conditions. Thus, in the liquid state, reduced and calcined Au/TiO_2 exhibits different behavior. Although the particle size in the calcined samples was rather stable, the reduced catalysts changed considerably.

Different particle structures caused the different behaviors, as revealed by phase-contrast STEM micrographs. After pretreatment in H_2 at elevated temperature, the Au particles were polycrystalline with multiple twin morphology, whereas the calcined catalysts generally contained Au single crystals. The EXAFS data also show the polycrystallinity of the reduced Au particles. The coordination number revealed a particle size of 2.1 nm before reaction and 1.4 nm after reaction.

The formation of multiple twinned particles (MTPs) on one hand and single crystals on the other was caused by different degrees of interaction between Au and TiO_2. On weakly interacting supports such as carbon, MTPs form preferentially,[96] as is also the case in inert atmosphere such as argon.[97] In contrast, single crystals form on strongly interacting supports such as MgO because the strong interaction forces the particles to maximize their common surface with the support.[91] Accordingly, reduction led to a weak interaction between Au and TiO_2, whereas calcination in air strongly increases the interaction[98] and fcc single crystals are formed.

Leaching does not explain the formation of small particles under the reaction conditions. Leaching of Au (about 8%) occurred, but this is not nearly enough to generate the small particles.

An additional experiment showed that a redispersion mechanism, driven by dissolution of Au and redeposition on the catalyst surface, can be excluded. In this experiment, two PEEK plates were placed in the reaction mixture at fixed positions. One PEEK plate was coated with Au/TiO_2, and the other, with TiO_2. If redispersion occurs in the liquid phase, then deposition of Au on TiO_2 would be observed by electron microscopy after the reaction. This was not the case.

Since there was redispersion in the THF and toluene solvents without a substrate, it is concluded that the redispersion does not depend on the catalytic reaction; however, an effect of the ligand cannot be excluded. The interaction of 4-nitrobenzaldehyde and benzaldehyde with the catalyst surface seem to hinder or slow down the breakup of Au particles. The amino group, on the other hand, does not seem to hinder redispersion and may even promote it. Prasad et al.,[42] for example, reported that amines, as well as thiols, silanes, and phosphines, act as surface-active ligands and convert polydispersed gold colloids with particles up to a few hundred nanometers to nearly monodisperse particles between 5 and 9 nm.

A possible mechanism for Au redispersion, which may also apply in this case, has been reported by Romero-Sarria et al.,[37,38] who state that gold particles in a Au/CeO_2 catalyst doped with 10% Eu preferentially interacted with the support across oxygen vacancies because this interaction is energetically favored. They found that as the presence of oxygen vacancies increased when the catalyst was treated with H_2, Au crystallites broke apart and migrated to the oxygen vacancies. When the atmosphere was changed to synthetic air, the redispersion was reversed, as indicated by reappearing diffraction peaks of metallic Au in the XRD spectra. They concluded that the reason for the redispersion was due to the stronger interaction of Au with the support across oxygen vacancies compared with the gold−gold interaction. They further concluded that the reverse process (sintering) in the presence of air occurred because the gold−gold interaction is stronger than the gold-support interaction when the energetically favorable gold-support interaction across oxygen vacancies stops. In our case, too, additional oxygen vacancies may form under the reaction conditions, and these vacancies may act as preferential anchor sites for Au and cause the redispersion.

Finally, the fact that MTPs are strained particles might also play a role in their breakup. They are composed of slightly distorted tetrahedral segments joined along twin boundaries forming a 5-fold symmetry axis. There are two basic forms: decahedral particles made up of five subunits, and icosahedral particles made up of 20 tetrahedral subunits.[89] However,

tetrahedral segments joined in this way do not fill the space completely.[99] The resulting solid angle deficiency is compensated for by a disclination, resulting in an inhomogeneous strain throughout the particle.[100−102] The particles after reduction in H_2 may not be in thermodynamic equilibrium and may reach an energetically more stable state by redispersion under the reaction conditions.

In summary, under the applied reaction conditions, large Au particles broke apart and formed active small particles. This study illustrates the complex interaction of Au particles with TiO_2 and their dynamic changes under varying conditions.

CONCLUSIONS

Electron microscopy and EXAFS measurements at the Au L_3 edge revealed dynamic changes in the dispersion of Au nanoparticles in Au/TiO_2 catalysts in the liquid phase under reducing conditions, depending on the applied gas-phase pretreatment of the catalyst. Large polycrystalline Au particles with a mean size of around 9 nm formed during reduction in H_2 at 60 to 300 °C, indicating a weak interaction of Au and the support. EXAFS measurements indicated that the Au particles observed by electron microscopy may be aggregates of smaller particles. In contrast, calcination between 300 and 500 °C led to a strong interaction between Au and TiO_2, which mainly led to the formation Au single crystals with an average size between 4 and 5 nm. After the reductive pretreatment, the multiple-twinned Au particles were unstable and broke apart, forming significant numbers of Au particles smaller than 2 nm. No redispersion was observed for calcined Au/TiO_2. As a result of the strong metal−support interaction, the large single-crystal Au particles in these catalysts were more or less stable under the reaction conditions.

AUTHOR INFORMATION

Corresponding Author

*Phone: +41 44 632 55 42. Fax: +41 44 633 12 52. E-mail: jeroen.vanbokhoven@chem.ethz.ch.

Notes

The authors declare no competing financial interest.

ACKNOWLEDGMENTS

The authors thank the electron microscopy center of ETH Zurich (EMEZ) for providing measurement time, the PSI in Switzerland for providing beamtime at the SuperXAS, Prof. Christopher Hardacre and Dr. Hermann Emerich for valubable discussions and conduction of additional experiments, and Marcia Schönberg for careful reading of the manuscript.

REFERENCES

(1) Bartholomew, C. H. In *Catalysis*; Specialist Periodical Report; House, Thomas Graham, Ed.; Royal Society of Chemistry: Cambridge, 1992; Vol. *10*, p 41.
(2) Lieske, H.; Lietz, G.; Spindler, H.; Voelter, J. *J. Catal.* **1983**, *81*, 8−16.
(3) Lietz, G.; Lieske, H.; Spindler, H.; Hanke, W.; Voelter, J. *J. Catal.* **1983**, *81*, 17−25.
(4) Birgersson, H.; Eriksson, L.; Boutonnet, M.; Järås, S. G. *Appl. Catal., B* **2004**, *54*, 193−200.
(5) Galisteo, F. C.; Mariscal, R.; Granados, M. L. p.; Fierro, J. L. G.; Daley, R. A.; Anderson, J. A. *Appl. Catal., B* **2005**, *59*, 227−233.
(6) Daley, R. A.; Christou, S. Y.; Efstathiou, A. M.; Anderson, J. A. *Appl. Catal., B* **2005**, *60*, 117−127.
(7) Hatanaka, M.; Takahashi, N.; Tanabe, T.; Nagai, Y.; Dohmae, K.; Aoki, Y.; Yoshida, T.; Shinjoh, H. *Appl. Catal., B* **2010**, *99*, 336−342.
(8) Sushumna, I.; Ruckenstein, E. *J. Catal.* **1988**, *109*, 433−462.
(9) Calvin H, B.; Bartholomew, C. H.; Fuentes, G. A. *Stud. Surf. Sci. Catal.* **1997**, *111*, 585−592.
(10) Baker, R. T.; Bartholomew, C. H.; Dadyburjor, D. B. In *Stability of Supported Catalysts: Sintering and Redispersion*; Horsley, J. A., Ed.; Catalytica, 1991.
(11) Calvin H, B. *Appl. Catal., A* **1993**, *107*, 1−57.
(12) Le Normand, F.; Borgna, A.; Garetto, T. F.; Apesteguia, C. R.; Moraweck, B. *J. Phys. Chem.* **1996**, *100*, 9068−9076.
(13) Fiedorow, R. M. J.; Wanke, S. E. *J. Catal.* **1976**, *43*, 34−42.
(14) Stulga, J. E.; Wynblatt, P.; Tien, J. K. *J. Catal.* **1980**, *62*, 59−69.
(15) Straguzzi, G. I.; Aduriz, H. R.; Gigola, C. E. *J. Catal.* **1980**, *66*, 171−183.
(16) Foger, K.; Jaeger, H. *J. Catal.* **1985**, *92*, 64−78.
(17) Lee, T. J.; Kim, Y. G. *J. Catal.* **1984**, *90*, 279−291.
(18) Lamber, R.; Romanowski, W. *J. Catal.* **1987**, *105*, 213−226.
(19) Newton, M. A.; Belver-Coldeira, C.; Martinez-Arias, A.; Fernandez-Garcia, M. *Nat. Mater.* **2007**, *6*, 528−532.
(20) Chen, J. J.; Ruckenstein, E. *J. Phys. Chem.* **1981**, *85*, 1606−1612.
(21) Ruckenstein, E.; Chen, J. J. *J. Colloid Interface Sci.* **1982**, *86*, 1−11.
(22) Van't Blik, H. F. J.; Van Zon, J. B. A. D.; Huizinga, T.; Vis, J. C.; Koningsberger, D. C.; Prins, R. *J. Am. Chem. Soc.* **1985**, *107*, 3139−3147.
(23) Bernal, S.; Botana, F. J.; Calvino, J. J.; Cifredo, G. A.; Pérez-Omil, J. A.; Pintado, J. M. *Catal. Today* **1995**, *23*, 219−250.
(24) Bernal, S.; Calvino, J. J.; Cauqui, M. A.; Pérez-Omil, J. A.; Pintado, J. M.; Rodríguez-Izquierdo, J. M. *Appl. Catal., B* **1998**, *16*, 127−138.
(25) Van't Blik, H. F. J.; Van Zon, J. B. A. D.; Koningsberger, D. C.; Prins, R. *J. Mol. Catal.* **1984**, *25*, 379−396.
(26) Grunwaldt, J.-D.; Basini, L.; Clausen, B. S. *J. Catal.* **2001**, *200*, 321−329.
(27) Wang, T.; Schmidt, L. D. *J. Catal.* **1981**, *70*, 187−197.
(28) Weststrate, C.; Hauman, M.; Moodley, D.; Saib, A.; van Steen, E. *Top. Catal.* **2011**, *54*, 811−816.
(29) Potoczna-Petru, D.; Jablonski, J. M.; Okal, J.; Krajczyk, L. *Appl. Catal., A* **1998**, *175*, 113−120.
(30) Potoczna-Petru, D.; Kepinski, L. *Catal. Lett.* **1991**, *9*, 355−362.
(31) Chernavskii, P. A.; Pankina, G. V.; Zaikovskii, V. I.; Peskov, N. V.; Afanasiev, P. *J. Phys. Chem. C* **2008**, *112*, 9573−9578.
(32) Ruckenstein, E.; Lee, S. H. *J. Catal.* **1984**, *86*, 457−464.
(33) Ruckenstein, E.; Hu, X. D. *Langmuir* **1985**, *1*, 756−760.
(34) Nakayama, T.; Arai, M.; Nishiyama, Y. *J. Catal.* **1983**, *79*, 497−500.
(35) Shimizu, K.-i.; Katagiri, M.; Satokawa, S.; Satsuma, A. *Appl. Catal., B* **2011**, *108−109*, 39−46.
(36) Breen, J. P.; Burch, R.; Hardacre, C.; Hill, C. J.; Krutzsch, B.; Bandl-Konrad, B.; Jobson, E.; Cider, L.; Blakeman, P. G.; Peace, L. J.; Twigg, M. V.; Preis, M.; Gottschling, M. *Appl. Catal., B* **2007**, *70*, 36−44.
(37) Romero-Sarria, F.; Martínez T, L. M.; Centeno, M. A.; Odriozola, J. A. *J. Phys. Chem. C* **2007**, *111*, 14469−14475.
(38) Hernández, W. Y.; Romero-Sarria, F.; Centeno, M. A.; Odriozola, J. A. *J. Phys. Chem. C* **2010**, *114*, 10857−10865.
(39) Deng, W.; Frenkel, A. I.; Si, R.; Flytzani-Stephanopoulos, M. *J. Phys. Chem. C* **2008**, *112*, 12834−12840.
(40) Goguet, A.; Hardacre, C.; Harvey, I.; Narasimharao, K.; Saih, Y.; Sa, J. *J. Am. Chem. Soc.* **2009**, *131*, 6973−6975.
(41) Sá, J.; Goguet, A.; Taylor, S. F. R.; Tiruvalam, R.; Kiely, C. J.; Nachtegaal, M.; Hutchings, G. J.; Hardacre, C. *Angew. Chem., Int. Ed.* **2011**, *50*, 8912−8916.
(42) Prasad, B. L. V.; Stoeva, S. I.; Sorensen, C. M.; Klabunde, K. J. *Chem. Mater.* **2003**, *15*, 935−942.
(43) Guzman, J.; Gates, B. C. *Angew. Chem., Int. Ed.* **2003**, *42*, 690−693.
(44) Guzman, J.; Gates, B. C. *J. Catal.* **2004**, *226*, 111−119.

(45) Zhang, X.; Shi, H.; Xu, B.-Q. *Angew. Chem., Int. Ed.* **2005**, *44*, 7132−7135.
(46) Zhang, X.; Shi, H.; Xu, B.-Q. *Catal. Today* **2007**, *122*, 330−337.
(47) Zhang, X.; Llabrés i Xamena, F. X.; Corma, A. *J. Catal.* **2009**, *265*, 155−160.
(48) Guan, Y.; Hensen, E. J. M. *Phys. Chem. Chem. Phys.* **2009**, *11*, 9578−9582.
(49) Choudhary, T. V.; Sivadinarayana, C.; Datye, A. K.; Kumar, D.; Goodman, D. W. *Catal. Lett.* **2003**, *86*, 1−8.
(50) Lopez-Sanchez, J. A.; Lennon, D. *Appl. Catal., A* **2005**, *291*, 230−237.
(51) Segura, Y.; López, N.; Pérez-Ramírez, J. *J. Catal.* **2007**, *247*, 383−386.
(52) Smirnov, S. A.; Smirnov, V. V. *Gold Bull.* **2009**, *42*, 182−189.
(53) Bailie, J. E.; Hutchings, G. J. *Chem. Commun.* **1999**, 2151−2152.
(54) Zanella, R.; Louis, C.; Giorgio, S.; Touroude, R. *J. Catal.* **2004**, *223*, 328−339.
(55) Claus, P. *Appl. Catal., A* **2005**, *291*, 222−229.
(56) Bus, E.; Prins, R.; van Bokhoven, J. A. *Catal. Commun.* **2007**, *8*, 1397−1402.
(57) Corma, A.; Serna, P. *Science* **2006**, *313*, 332−334.
(58) Corma, A.; Concepción, P.; Serna, P. *Angew. Chem., Int. Ed.* **2007**, *46*, 7266−7269.
(59) Cárdenas-Lizana, F.; Gómez-Quero, S.; Perret, N.; Keane, M. A. *Gold Bull.* **2009**, *42*, 124−132.
(60) Mavrikakis, M.; Stoltze, P.; Nørskov, J. K. *Catal. Lett.* **2000**, *64*, 101−106.
(61) Overbury, S. H.; Schwartz, V.; Mullins, D. R.; Yan, W.; Dai, S. *J. Catal.* **2006**, *241*, 56−65.
(62) Brodersen, S. H.; Grønbjerg, U.; Hvolbæk, B.; Schiøtz, J. *J. Catal.* **2011**, *284*, 34−41.
(63) Valden, M.; Lai, X.; Goodman, D. W. *Science* **1998**, *281*, 1647−1650.
(64) Haruta, M. *Catal. Today* **1997**, *36*, 153−166.
(65) Fujitani, T.; Nakamura, I.; Akita, T.; Okumura, M.; Haruta, M. *Angew. Chem., Int. Ed.* **2009**, *48*, 9515−9518.
(66) Bond, G. *Gold Bull.* **2010**, *43*, 88−93.
(67) Corma, A.; Serna, P.; Garcia, H. *J. Am. Chem. Soc.* **2007**, *129*, 6358−6359.
(68) Santos, L. L.; Serna, P.; Corma, A. *Chem.—Eur. J.* **2009**, *15*, 8196−8203.
(69) Grirrane, A.; Corma, A.; Garcia, H. *Science* **2008**, *322*, 1661−1664.
(70) Grirrane, A.; Corma, A.; Garcia, H. *Nat. Protoc.* **2010**, *11*, 429−438.
(71) Cárdenas-Lizana, F.; Gómez-Quero, S.; Keane, M. A. *ChemSusChem* **2008**, *1*, 215−221.
(72) Shimizu, K.-i.; Miyamoto, Y.; Kawasaki, T.; Tanji, T.; Tai, Y.; Satsuma, A. *J. Phys. Chem. C* **2009**, *113*, 17803−17810.
(73) Zanella, R.; Louis, C.; Giorgio, S.; Touroude, R. *J. Catal.* **2004**, *223*, 328−339.
(74) Boronat, M.; Concepción, P.; Corma, A.; González, S.; Illas, F.; Serna, P. *J. Am. Chem.* **2007**, *129*, 16230−16237.
(75) Panayotov, D. A.; Yates, J. T. *J. Phys. Chem. C* **2007**, *111*, 2959−2964.
(76) Molina, L. M.; Alonso, J. A. *J. Phys. Chem. C* **2007**, *111*, 6668−6677.
(77) Boronat, M.; Illas, F.; Corma, A. *J. Phys. Chem. A* **2009**, *113*, 3750−3757.
(78) Boronat, M.; Concepción, P.; Corma, A. *J. Phys. Chem. C* **2009**, *113*, 16772−16784.
(79) Nakamura, I.; Mantoku, H.; Furukawa, T.; Fujitani, T. *J. Phys. Chem. C* **2011**, *115*, 16074−16080.
(80) Panayotov, D. A.; Burrows, S. P.; Yates, J. T.; Morris, J. R. *J. Phys. Chem. C* **2011**, *115*, 22400−22408.
(81) Borchert, H.; Shevchenko, E. V.; Robert, A.; Mekis, I.; Kornowski, A.; Gruebel, G.; Weller, H. *Langmuir* **2005**, *21*, 1931−1936.
(82) Zanella, R.; Louis, C. *Catal. Today* **2005**, *107−108*, 768−777.
(83) Krumeich, F.; Müller, E.; Wepf, R. A.; Nesper, R. *J. Phys. Chem. C* **2011**, *115*, 1080−1083.
(84) Nellist, P. D.; Pennycook, S. J. *Science* **1996**, *247*, 413−415.
(85) de Graaf, J.; van Dillen, A. J.; de Jong, K. P.; Koningsberger, D. C. *J. Catal.* **2001**, *203*, 307−321.
(86) Richner, G.; van Bokhoven, J. A.; Neuhold, Y.-M.; Makosch, M.; Hungerbuehler, K. *Phys. Chem. Chem. Phys.* **2011**, *13*, 12463−12471.
(87) Hofmeister, H. *Cryst. Res. Technol.* **1998**, *33*, 3−25.
(88) Mativetsky, J. M.; Fostner, S.; Burke, S. A.; Grutter, P. *Phys. Rev. B* **2009**, *80*, 045430.
(89) Ino, S. *J. Phys. Soc. Jpn.* **1969**, *27*, 941−953.
(90) Iijima, S.; Ichihashi, T. *Phys. Rev. Lett.* **1986**, *56*, 616−619.
(91) Zhang, B.; Wang, D.; Zhang, W.; Su, D. S.; Schlögl, R. *Chem.—Eur. J.* **2011**, *17*, 12877−12881.
(92) Bus, E.; Prins, R.; van Bokhoven, J. A. *Phys. Chem. Chem. Phys.* **2007**, *9*, 3312−3320.
(93) Matthey, D.; Wang, J. G.; Wendt, S.; Matthiesen, J.; Schaub, R.; Laegsgaard, E.; Hammer, B.; Besenbacher, F. *Science* **2007**, *315*, 1692−1696.
(94) Wu, T.; Kaden, W. E.; Anderson, S. L. *J. Phys. Chem. C* **2008**, *112*, 9006−9015.
(95) Manuscript in preparation.
(96) Ogawa, S.; Ino, S.; Kato, T.; Ota, H. *J. Phys. Soc. Jpn.* **1966**, *21*, 1963−1972.
(97) Kimoto, K.; Nishida, I. *J. Phys. Soc. Jpn.* **1967**, *22*, 940.
(98) Haruta, M.; Daté, M. *Appl. Catal., A* **2001**, *222*, 427−437.
(99) Nepijko, S. A.; Styopkin, V. I.; Hofmeister, H.; Scholtz, R. *J. Cryst. Growth* **1986**, *76*, 501−506.
(100) Johnson, C. L.; Snoeck, E.; Ezcurdia, M.; Rodríguez-González, B.; Pastoriza-Santos, I.; Liz-Marzán, L. M.; Hÿtch, M. J. *Nat. Mater.* **2007**, *7*, 120−124.
(101) Johnson, C. L.; Snoeck, E.; Hÿtch, M. J. *Microsc. Microanal.* **2010**, *16*, 1782−1783.
(102) Johnson, C. L.; Snoeck, E.; Ezcurdia, M.; Rodriguez-Gonzalez, B.; Pastoriza-Santos, I.; Liz-Marzan, L. M.; Hytch, M. J. *Nat. Mater.* **2008**, *7*, 120−124.